

# Galaxy Population in a Cluster of Galaxies around the Radio Galaxy 3C 324 at $z = 1.2$ <sup>1</sup>

Fumiaki NAKATA,<sup>2</sup> Masaru KAJISAWA,<sup>3</sup> Toru YAMADA,<sup>4</sup> Tadayuki KODAMA,<sup>2</sup>  
Kazuhiro SHIMASAKU,<sup>2</sup> Ichi TANAKA,<sup>4</sup> Mamoru DOI,<sup>5</sup> Hisanori FURUSAWA,<sup>2</sup>  
Masaru HAMABE,<sup>6</sup> Masanori IYE,<sup>4</sup> Masahiko KIMURA,<sup>7</sup> Yutaka KOMIYAMA,<sup>8</sup>  
Satoshi MIYAZAKI,<sup>4</sup> Sadanori OKAMURA,<sup>2</sup> Masami OUCHI,<sup>2</sup> Toshiyuki SASAKI,<sup>8</sup>  
Maki SEKIGUCHI,<sup>7</sup> Masafumi YAGI,<sup>4</sup> and Naoki YASUDA<sup>4</sup>

<sup>2</sup>*Department of Astronomy, School of Science, The University of Tokyo, Bunkyo-ku, Tokyo 113-0033  
nakata@astron.s.u-tokyo.ac.jp*

<sup>3</sup>*Astronomical Institute, Tohoku University, Aoba-ku, Sendai, Miyagi 980-8578*

<sup>4</sup>*National Astronomical Observatory of Japan, 2-21-1 Osawa, Mitaka, Tokyo 181-8588*

<sup>5</sup>*Institute of Astronomy, The University of Tokyo, Mitaka, Tokyo 181-1500*

<sup>6</sup>*Department of Mathematical and Physical Sciences, Faculty of Science,  
Japan Women's University, 2-8-1 Mejirodai, Bunkyo-ku, Tokyo 112-8681*

<sup>7</sup>*Institute for Cosmic Ray Research, The University of Tokyo, 5-1-5 Kashiwa-no-Ha, Kashiwa,  
Chiba 277-8582*

<sup>8</sup>*Subaru Telescope, National Astronomical Observatory of Japan, 650 North Aohoku Place, Hilo,  
HI 96720, U.S.A*

(Received 2001 May 28; accepted 2001 September 25)

## Abstract

We discuss the properties of galaxies around the radio galaxy 3C 324 at  $z = 1.2$  based on *BVRIC'* multi-band imaging data. We have applied a photometric-redshift technique to objects in the 3C 324 field, and identified 35 objects as plausible cluster members. We have found that red and luminous members are concentrated in a small region enclosed by a circle of  $40''$  radius (0.33 Mpc at  $z = 1.2$  for  $\Omega_0 = 0.3$ ,  $\lambda_0 = 0.7$ ,  $H_0 = 70 \text{ km s}^{-1} \text{ Mpc}^{-1}$  cosmology) from the 3C 324 galaxy. The 3C 324 cluster is probably much more compact in size compared with the local clusters. We constructed a *K'*-band luminosity function of the cluster members and fit a Schechter function, and found the characteristic magnitude to be  $K'_{AB} = 20.2 \pm 0.6$ . This value is consistent with the extrapolation of the pure passive evolution seen for  $z < 1$  clusters. We have identified eight bright galaxies which form a red color-magnitude sequence. The slope of the sequence is consistent with the passive evolution model down to  $K'_{AB} < 22$ ; we also found that there is no clear age variation in these bright red galaxies. However, seven out of these eight galaxies exhibit a significant excess in the rest UV light with respect to the passive evolution model. This may suggest that the massive early-type galaxies in this high-redshift cluster are still forming stars to some extent. We have confirmed a truncation of the color-magnitude sequence at  $K'_{AB} \sim 22$ ; faint passively-evolving galaxies may not yet be present in this cluster at  $z \sim 1.2$ . The overall color distribution of the cluster members, selected by the photometric redshift technique, is found to be very broad. We derived the fraction of blue galaxies in this cluster following a definition of Butcher and Oemler (1984), and obtained  $f_B = 0.39 \pm 0.28$ , which is higher than that for  $z < 1$  clusters. This indicates that the star-formation activity of this cluster is, on the average, higher than that of lower redshift counterparts.

**Key words:** galaxies: clusters: individual (3C 324) — galaxies: elliptical and lenticular, cD — galaxies: evolution — galaxies: formation — galaxies: luminosity function, mass function

## 1. Introduction

The early evolution of early-type (elliptical and S0) galaxies can provide a strong constraint on galaxy-formation models. Because early type galaxies form the dominant population in nearby rich clusters (Oemler 1974; Dressler 1980), they are very efficiently studied in clusters. According to many important observations made for clusters at  $z \lesssim 1$ , it is well established that the majority of the early-type galaxies observed in nearby and intermediate-redshift ( $z \sim 0.5$ ) clusters mainly consist of old stellar

populations formed at high redshifts ( $z_F > 2$ , e.g., O'Connell 1988; Bower et al. 1992; Aragón-Salamanca et al. 1993; Rakos, Schombert 1995; Gladders et al. 1998; Ellis et al. 1997; Stanford et al. 1998; Kodama et al. 1998).

On the other hand, there are also many pieces of evidence suggesting that the evolution of the entire cluster galaxy population is not as simple as expected from the monolithic galaxy formation scenario. It is known that the fraction of blue galaxies in clusters increases rapidly with the redshift at  $z \lesssim 1$  (Butcher, Oemler 1978, 1984; Rakos, Schombert 1995). Through previous spectroscopic

<sup>1</sup> Based in part on data collected at Subaru Telescope, which is operated by the National Astronomical Observatory of Japan.

studies of intermediate-redshift clusters, it is also known that a significant fraction of galaxies have emission-lines and/or post-starburst signatures (e.g., Dressler, Gunn 1992; Postman et al. 1998; Dressler et al. 1999; Poggianti et al. 1999). Such blue and star-forming galaxies are notably rare in rich clusters at  $z \sim 0$ . Recent ground-based spectroscopic observation and Hubble Space Telescope (HST) high-resolution imaging have further revealed a population of old galaxies with ongoing or recent (within a few Gyr prior to the observation) star-formation activity as well as a significantly large fraction of late-type disk galaxies and closely interacting systems in intermediate redshift clusters (Abraham et al. 1996; Morris et al. 1998; Oemler et al. 1997; Couch et al. 1998; van Dokkum et al. 1998; Poggianti et al. 1999). This star-forming activity of cluster galaxies is possibly related to the evolution of the morphological mix of the cluster galaxy populations, particularly, the origin of S0 galaxies (Dressler et al. 1997; van Dokkum et al. 1998, 2000; Kuntschner, Davis 1998). As a natural extension of these results, it is expected that a stronger evolution of galaxies may be observed in clusters at higher redshifts.

Recently, more than several clusters and cluster candidates have been discovered at  $z \gtrsim 1$  (Dickinson 1995; Postman et al. 1996; Stanford et al. 1997; Hall, Green 1998; Ostrander et al. 1998; Olsen et al. 1999; Benítez et al. 1999; Rosati et al. 1999; Tanaka et al. 2000; Best 2000). By observing higher-redshift clusters, any difference in the star-forming history can be seen more clearly. A rapid change in the colors of passively evolving galaxies only occurs within  $\sim 2\text{--}3$  Gyr after the end of the star formation (e.g., Bower et al. 1992, 1998). If cluster early-type galaxies formed at  $z > 2$  and evolved passively, one can expect conspicuous color changes only at  $z \gtrsim 1$ . One may also expect more frequent star-formation activity at higher redshifts, since there are a significant fraction of galaxies with poststarburst signatures in intermediate-redshift clusters (Couch, Sharples 1987; Dressler, Gunn 1992; Barger et al. 1996; Postman et al. 1998; Couch et al. 1998; Poggianti et al. 1999). A simple extrapolation of the Butcher–Oemler effect (Butcher, Oemler 1984) also predicts a blue galaxy fraction greater than 50% at  $z \sim 1$ . It is therefore interesting to extend the detailed color analysis to other clusters at  $z \gtrsim 1$ , and to probe the early history of star formation in clusters.

To date, however, only a few clusters at  $z \gtrsim 1$  have been studied in detail by multicolor photometry (Stanford et al. 1997; Benítez et al. 1999; Rosati et al. 1999; Tanaka et al. 2000; Haines et al. 2001; van Dokkum et al. 2001). The two largest difficulties in studying the galaxy population in these high-redshift clusters are: (1) the faintness of the cluster galaxies due to the large distance from us and (2) contamination of the foreground and the background galaxies, as they tend to dominate the galaxy surface number density on the sky towards the high redshift clusters. We have overcome these difficulties by utilizing the huge light-collecting power of the 8 m Subaru telescope and by applying a photometric-redshift technique to isolate the possible cluster members.

We discuss in this paper the 3C 324 cluster at  $z = 1.2$ . An excess of galaxy surface number density in this region was recognized by Kristian, Sandage, and Katem (1974) and by Spinrad and Djorgovski (1984), and firmly identified by Dickinson (1995). In Dickinson’s (1997b) spectroscopic study, the surface-density excess was revealed to be due to the presence of two clusters or rich groups at  $z = 1.15$  and  $z = 1.21$ . Extended X-ray emission with a luminosity comparable to that of the Coma cluster has been detected in the direction of 3C 324 (Dickinson 1997a), which suggests that at least one of the two systems is a collapsed massive system. From a deep HST image, Smail and Dickinson (1995) detected a weak shear pattern in the field that may be produced by a cluster. In the following discussion, we do not distinguish the two clusters at  $z \sim 1.2$ , since either a detailed redshift distribution of the galaxies or the relative population of the two systems is not yet available. We thus discuss the average properties of the two clusters. Since their redshifts are close to each other, this has little effect on our discussion about the luminosity and color distributions.

The 3C 324 cluster has been studied by Kajisawa et al. (2000a,b; hereinafter referred to as K00a,b) with the HST  $B_{F450W}$ - and  $R_{F702W}$ -bands and the Subaru  $K'$ -band data, which we include in this analysis as well. K00a investigated the  $K'$ -band luminosity distribution of galaxies around 3C 324. They found an abrupt decrease in the  $K'$ -band luminosity function for galaxies in the cluster core region ( $< 40''$  from 3C 324) at  $K'_{AB} \gtrsim 22$ , and suggested two possible interpretations, namely, luminosity segregation where a fraction of bright galaxies increases toward the cluster center, or the intrinsic deficiency of faint galaxies in the 3C 324 cluster. K00b also studied the optical and near-infrared color of  $K'$ -selected galaxies in this cluster. They found a truncation of the color–magnitude sequence of the 3C 324 cluster at  $K'_{AB} \sim 22$ . They also argued that the bulge-dominated galaxies in the field seem to form a broad sequence in the color–magnitude diagram, whose slope at the faint end is much steeper than that expected from metallicity variations within a passively evolving co-eval galaxy population.

These results, however, are based on simple color selection or statistical background subtraction of the field galaxies, and can be affected by a contamination of the foreground/background objects. It is clearly needed to test them using a sample of galaxies that are more firmly identified as cluster members.

Spectroscopic redshifts are ideal, but not practical, at this high redshifts ( $z > 1$ ), since even with 2 hours of integration on an 8 m-class telescope, we can reach only down to  $\sim M^*$ . Therefore, it is extremely time-consuming to make a complete sample over a representative field of distant clusters (e.g., 1 Mpc). In this paper, we try to overcome this difficulty in identifying cluster membership by using a photometric-redshift technique. This approach enables us to investigate the galaxy properties of likely cluster members; importantly, not only for the galaxies on the red sequence, but also for relatively blue galaxies, which are otherwise embedded in numerous field popula-

tions on a color–magnitude diagram. For this purpose, we newly obtained  $V$  and  $I$  data with Suprime-Cam at the Cassegrain focus of the Subaru telescope.

Firstly, we made a catalog of  $K'$ -band selected objects. The use of a  $K'$ -band sample has the following two advantages. First, the selection bias at large redshifts is small, and thus a direct comparison with lower-redshift clusters is possible (Aragón-Salamanca et al. 1993). Second, the sample selection is less affected by the star-formation activity. We applied a photometric-redshift technique by utilizing multi-band imaging data, and identified 35 objects as plausible cluster members. With this new cluster membership information as well as two additional colors essential for a population analysis, we revisited the issues which remain unsettled in K00a,b. With the photometric-redshift selected sample, we showed that an abrupt decrease in the faint end of the  $K'$ -band luminosity function in the cluster core region shown in K00a, which is mainly because the fraction of faint members relative to the bright members is lower in the core region than in the whole cluster, i.e., luminosity segregation; we also found that K00a regarded some faint members as non-members. The truncation of the color–magnitude sequence, indicated in K00b, was clearly identified in this work as well. However, the broad and tilted color–magnitude sequence argued in K00b is not completely recovered by the photometric-redshift selected sample used in this paper. In addition to these interesting results, we newly found a UV-excess in some early-type galaxies, and also derived the blue fraction of the 3C 324 cluster at  $z \sim 1.2$ .

This paper is structured as follows. We describe the observations and data reduction briefly in section 2. Section 3 describes the object detection and number counts. In section 4, we describe the photometric-redshift technique and its application to our data. In section 5, we consider the spatial distribution, luminosity function, color properties and the blue galaxy fraction of the member galaxies in the 3C 324 cluster. We summarize the main results in section 6.

Throughout this paper we use the following cosmological parameters:  $H_0 = 70 \text{ km s}^{-1} \text{ Mpc}^{-1}$ ,  $\Omega_0 = 0.3$  and  $\lambda_0 = 0.7$ , which gives a physical scale of  $8.30 \text{ kpc arcsec}^{-1}$  at the cluster redshift.

## 2. Data

The  $K'$ -band and HST  $B_{F450W}$ - and  $R_{F702W}$ -band images used in this paper were taken from K00a,b and Kajisawa and Yamada (1999). We newly took  $V$  and  $I$  data with the Subaru telescope, which are described in detail below.

### 2.1. Suprime-Cam $V$ - and $I$ -band Data

Suprime-Cam (Miyazaki et al. 1998) is a mosaic CCD camera designed for use at the prime focus of the Subaru telescope with a field of view (FOV) of  $30'\phi$ . It is equipped with three-edge butttable 2k-by-4k CCDs in a  $2 \times 5$  array, giving a total of  $8k \times 10k$  effective pixels with a pixel size of  $15 \mu\text{m}$ . Suprime-Cam covers an FOV of  $24' \times 30'$ , al-

**Table 1.** Log of the observations.

Date	Band	Exposure	Frames	Seeing
18/5/99	$I$	15 min	4	$0''.5$
19/5/99	$I$	15 min	2	$0''.6$
11/6/99	$V$	15 min	4	$0''.7$
12/6/99	$V$	15 min	4	$0''.7$

most the entire FOV of the F/1.86 prime focus, with a resolution of  $0''.2$  per pixel.

The 3C 324 field was observed in the  $V$ - and  $I$ -bands with a Suprime-Cam mounted on the Cassegrain focus of the Subaru telescope during test observation runs for commissioning of the Cassegrain focus in May–June 1999. The FOV of the F/12.2 Cassegrain focus is  $6'$  in diameter; its physical size is almost the same as that of the prime focus. Only six of the 10 CCDs, however, were ready at the time of the  $V$  and  $I$  observations. Accordingly, Suprime-Cam at the Cassegrain focus covered an FOV of  $4' \times 3'$  with a resolution of  $0''.03$  per pixel.

A log of the observations is given in table 1. The total integration times of  $V$ - and  $I$ -bands are 2 hr and 1.5 hr, respectively. The seeings of the combined image are  $\sim 0''.7$  for  $V$  and  $\sim 0''.6$  for  $I$ . The weather condition was stable during the  $V$ -band observation. The  $I$ -band images, however, were taken under poorer conditions. The sky was not photometric during the  $I$ -band observation.

Data reduction of each frame in a given band proceeded as follows. First, a bias value was determined for each row of a frame as the median of the overscan region. By subtracting the bias value from each row, an overscan-subtracted frame was made. Then, the median bias frame was made by taking the median of the available overscan-subtracted bias frames. This median bias frame, whose average DC level is zero, was subtracted from all of the overscan-subtracted frames so that the residual bias pattern would be eliminated. Since the temperature of the dewar of Suprime-Cam was not sufficiently low ( $\sim -75^\circ\text{C}$ ) and was unstable during the observations, the noise level due to dark currents was high and varied. Thus, a dark frame was created for each of the object frames, depending on the temperature of the dewar at the time when the frame was exposed.

Next, flatfielding was performed. Because the  $V$ -band images suffered from stray light, the flat-field frame for the  $V$ -band was made from twilight sky frames in which the counts of stray light were negligible. For the  $I$ -band, however, the flat-field frame was made from dome-flat frames, because twilight sky frames showed a strong fringe pattern. All of the frames were flat-fielded. Thus, the fringe frame was made by taking the median of the object frames; it was then subtracted from each of the flat-fielded object frames. Since the dome flat may not reflect the global pattern of the CCD sensitivity, we further corrected the  $I$ -band frame for the global sensitivity pattern. The sky flat frame was made by taking the median of the fringe-subtracted object frames. All of the object frames were flat-fielded again using this sky flat frame.

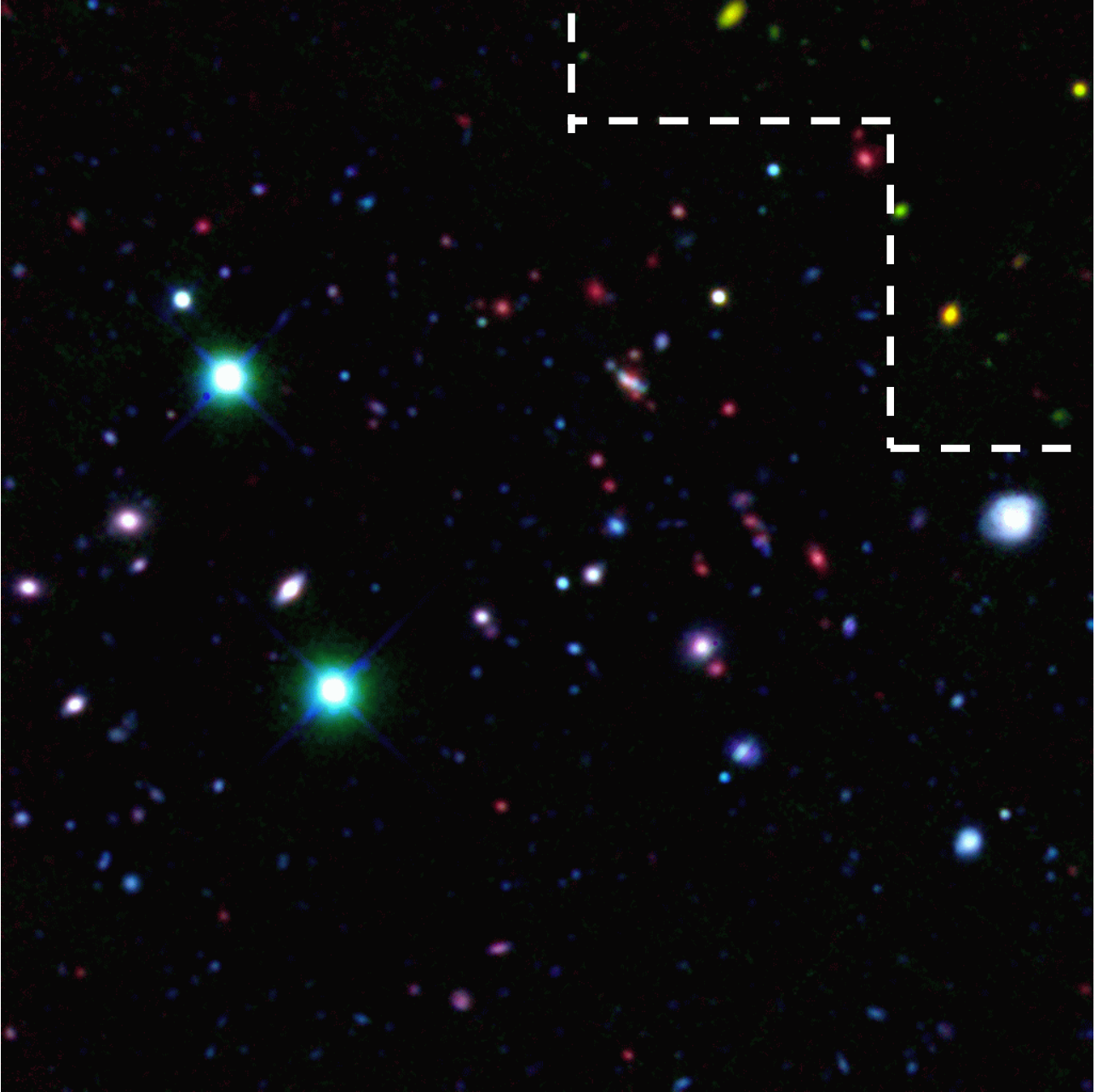


**Fig. 1.** Composite pseudo-color picture of the observed 3C 324 field. The RGB colors are assigned for  $K'$ ,  $I$ , and  $R_{F702W}$  images, respectively. The dashed line outlines the field of the HST observation; the upper-right region of the short-dashed line has not been observed with the HST.



The counts on those pixels contaminated with cosmic rays were replaced with values interpolated from the surroundings. Bad pixels were replaced with blanks, which were ignored in the following analysis.

After subtracting the local sky background level, defined by taking the median of the pixel values of the surrounding pixels, registering the relative positions of the dithered frames, and normalizing the sensitivity of the six chips, we finally co-added the individual exposures. We took the median in this process. We applied  $3 \times 3$  binning to obtain the final images in order to avoid over-sampling. The actual resolution of the final images is therefore  $0''.09$  per pixel.

For the  $V$ -band image, a flux calibration was performed using the Landolt (1992) standard stars taken during the observation. For the  $I$ -band image, which was not taken under the photometric condition, we used the HST image in the F791W band (exposure time of 1800 s, PI: M. Longair; PID: 1070) for the calibration. We acquired this F791W image from the HST Data Archive; the zero point was kindly provided by Best (2000). Although the transmission curves of the F791W filter and our  $I$ -band filter are slightly different, the color term was found to be negligible. We used 16 common objects in these two images to determine the zero-point of our  $I$ -band image. The standard deviation of F791W– $I$  colors of the 16 objects around the average F791W– $I$  value was only 0.037 mag.

## 2.2. CISCO $K'$ -band Data

$K'$ -band imaging of 3C 324 field was carried out with a near-infrared camera, CISCO (Motohara et al. 1998), mounted on the Cassegrain focus of the Subaru Telescope on 1999 March 31 and April 1, during the telescope commissioning period. The detector was a  $1024 \times 1024$  HAWAII HgCdTe array with a pixel scale of  $0''.116$ , which provided a field of view of  $\sim 2' \times 2'$ . Details concerning the reduction procedures are described in K00a. A flux calibration was performed by the UKIRT Faint Standard FS 27. The seeing size of the resultant frame was  $0''.8$ , which was measured from the FWHM of the stellar images.

## 2.3. HST $B_{F450W}$ and $R_{F702W}$ Data

The 3C 324 field was observed using the WFPC2 camera with a  $R$  (F702W) filter and a  $B$  (F450W) filter (PI: M. Dickinson; PIDs 5465 and 6553, respectively). These data were taken from the HST Data Archive. The total exposure times were 64800 s for the F702W image and 17300 s for the F450W image.

## 3. $K'$ -band Selected Sample

### 3.1. Object Detection and Photometry

We registered the  $B_{F450W}$ ,  $V$ ,  $R_{F702W}$ , and  $I$  images with the  $K'$  image, and applied Gaussian filters to smooth all of the images to  $\sim 0''.8$  resolution of the  $K'$  image. Only the region imaged with the CISCO is considered in the following analyses. A composite pseudo-color picture of the 3C 324 field is shown in figure 1, where the  $R$ ,  $G$ , and  $B$  colors are assigned for the stacked  $K'$ ,  $I$ , and  $R_{F702W}$

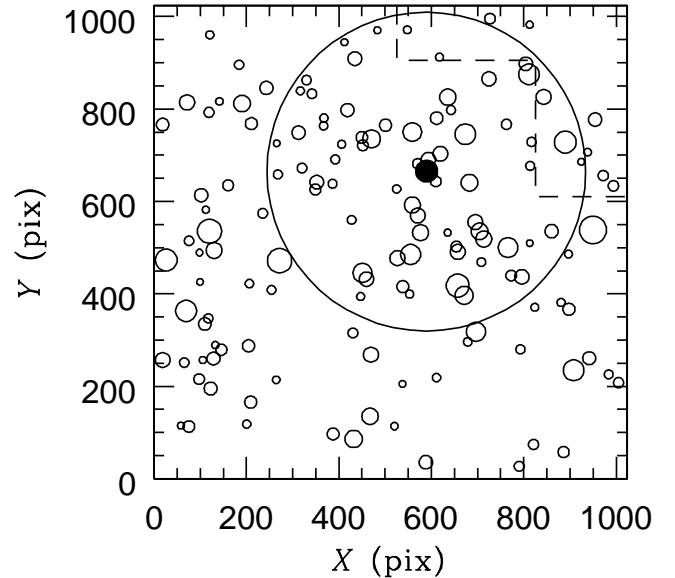


**Fig. 2.** Distribution of the 139 detected objects on the sky. 3C 324 is shown as the filled circle. The areas of the circles are in proportion to the brightness of objects. The dashed line outlines the field of the HST observation, similar to that shown in figure 1. The large circle indicates the ‘inner’ region within  $40''$  from 3C 324.

images, respectively. The dashed line outlines the field of the HST observation: the upper right region of the dashed line has not been observed with the HST.

Since the  $K'$ -band, whose effective wavelength is longer than  $4000\text{\AA}$  in the rest frame at  $z \sim 1.2$ , is essential for our photometric redshift analysis (Kodama et al. 1999), we first constructed a catalog of  $K'$ -band selected objects, and then searched for their counterparts on other optical frames. Object detection on the  $K'$ -band frame was carried out by the so-called ‘connected pixel method’. We defined an ‘object’ as a clump of more than  $N_{\min}$  connected pixels with counts larger than an isophotal threshold  $I_{\text{thres}}$ . In this study,  $I_{\text{thres}}$  was set to  $23.50 \text{ mag arcsec}^{-2}$ , which is  $\simeq 1.12$ -times the sky r.m.s. noise of the  $K'$ -band image;  $N_{\min}$  was set to 40 pixels ( $0.54 \text{ arcsec}^2$ ). Photometry was performed with an aperture having a radius of  $2r_{\text{Kron}}$ , where  $r_{\text{Kron}}$  is the Kron radius (See Metcalfe et al. 1991 for the definition) of the object. We did not apply any star/galaxy separation so as to avoid any possible omission of compact galaxies common at high redshifts; however, the star contamination is expected to be negligibly small at the faint magnitudes ( $K'_{\text{AB}} \gtrsim 19.5$ ) where we are mainly interested. A total of 139 sources were detected at magnitudes brighter than  $K'_{\text{AB}} = 24.0$ , which is the  $3\sigma$  detection limit of the  $K'$  image. Figure 2 shows the distribution of the detected objects on the sky. The areas of the circles are in proportion to the brightness of the detected objects. The filled circle indicates the position of the radio galaxy 3C 324. The large-circle shows a region of  $40''$  radius centered on 3C 324, which is discussed in subsection 5.1. The dashed line outlines the field of the HST observation, similar to that shown in

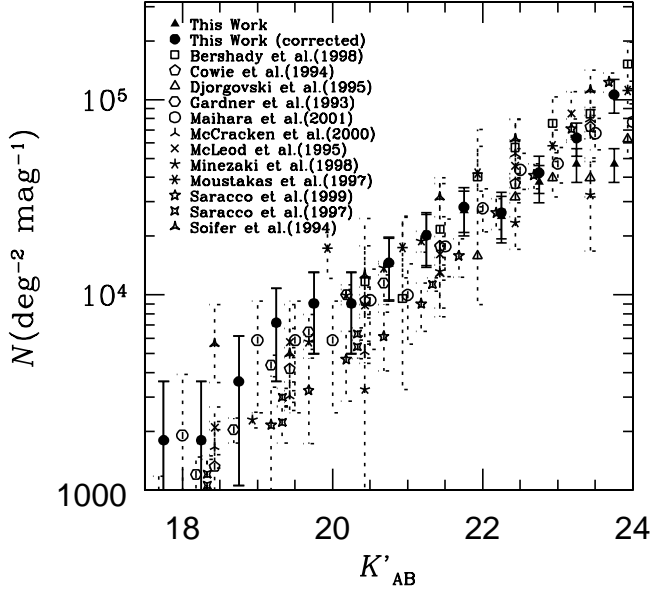


**Fig. 3.**  $K'$ -band number counts of the galaxies in the 3C 324 region. Filled triangles show raw counts, and filled circles indicate the counts corrected for incompleteness. Galaxy counts in the general field taken from various literature are also plotted using different symbols.

figure 1.

### 3.2. Number Counts

The differential number counts of galaxies detected on the entire field of the CISCO  $K'$ -band image are shown in figure 3. For a comparison, counts obtained in general fields taken from various literature are also shown. The filled triangles show our raw counts, and the filled circles indicate those counts corrected for incompleteness. The completeness of object detection as a function of the magnitude was adopted from K00a, who estimated the completeness factor at a given magnitude, using the IRAF ARTDATA package, by distributing a number of artificial objects of that magnitude on the observed frame, running the object detection software on the frame in the same manner as for real objects, and deriving the detection rate of the artificial objects.

The corrected counts of the 3C 324 field are consistent with those of the general fields within the error bars. Note, however, that the 3C 324 counts are slightly higher than the average of the general fields at  $19 < K'_{AB} < 22$ , which probably reflects the existence of the 3C 324 cluster. At  $K'_{AB} > 22$ , however, no apparent excess is seen. This abrupt decrease in the number count at the faint end may be due to a field variation, which is quite plausible for a small field coverage only  $2' \times 2'$  for the  $K'$ -image.

## 4. Photometric Redshift

To extract members of the 3C 324 cluster at  $z \sim 1.2$ , we applied a photometric-redshift technique to those objects with  $K'_{AB} < 24$ , which corresponds to the  $3\sigma$  detection

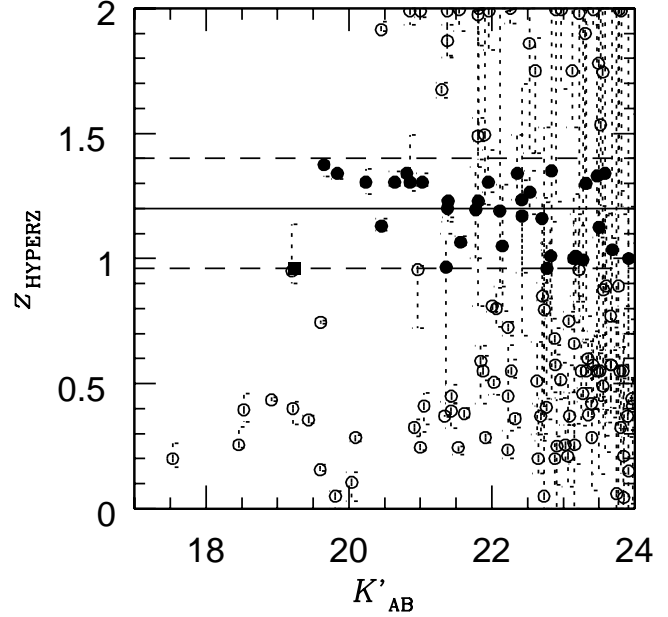


**Fig. 4.** Estimated photometric redshifts as a function of the  $K'_{AB}$  magnitude. The filled square shows 3C 324, and the filled circles indicate the cluster members, whose estimated photometric redshifts fall in the range  $z = 0.96\text{--}1.4$ . The error bars indicate the  $1\sigma$  errors, which are taken from outputs of the HYPERZ code.

limit of the  $K'$ -band image. We estimated the redshifts of these object using the HYPERZ code of Bolzonella, Miralles, and Pelló (2000). HYPERZ uses Bruzual and Charlot's (1993) stellar evolutionary code (GISEL98) to build synthetic template galaxies with 8 star-formation histories, which roughly match the observed properties of local galaxies from E to Im types: an instantaneous burst, a constant star-forming system, and six exponentially decaying SFRs with time-scales of from 1 to 30 Gyr. These models assume solar metallicity and a Millar–Scalo IMF, and internal reddening is considered using the Calzetti et al. (2000) model with  $A_V$  varying between 0 and 1.2 mag.

We used  $B_{F450W}$ ,  $V$ ,  $R_{F702W}$ ,  $I$  and  $K'$  bands to estimate the photometric redshifts, which covers from  $2060\text{\AA}$  ( $B_{F450W}$ ) to  $9721\text{\AA}$  ( $K'$ ) in the rest-frame effective wavelengths at a cluster redshift of 1.2. Because they properly bracket the  $4000\text{\AA}$  break with a sufficient number of bands, the photometric redshift estimation is expected to achieve a high performance (e.g., Kodama et al. 1999). However, since the colors of galaxies at  $z = 1.2$  in the  $R$ -,  $I$ -, and  $K'$ -bands are similar to those at the  $z > 2$ , some cluster members can be misidentified as  $z > 2$  galaxies. Therefore, we limit the range of the output redshifts from HYPERZ to  $0 \leq z \leq 2$ . That is, HYPERZ searches for the best-fit photometric redshifts of individual galaxies in the range  $0 \leq z \leq 2$ .

Figure 4 shows the estimated photometric redshifts as a function of the  $K'_{AB}$  magnitude. The filled square shows 3C 324. The error bars indicate the  $1\sigma$  errors, which are taken from outputs of the HYPERZ code. We find from figure 4 that  $\simeq 15$  galaxies with  $K'_{AB} \lesssim 22$  make a se-

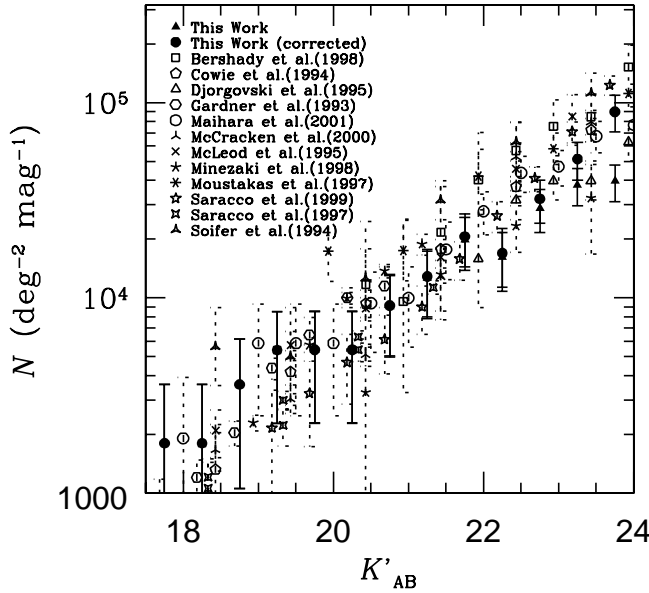


**Fig. 5.**  $K'$ -band number counts of galaxies in the 3C 324 field after removing the 35 cluster members. The symbols are the same as in figure 3.

quence around  $z \sim 1.2$ , which is near to the redshift of the 3C 324 cluster. Almost all of those galaxies, including 3C 324 (filled square), are distributed at  $0.96 \leq z \leq 1.4$ . Therefore, we decided to classify those galaxies whose estimated redshift is  $0.96 \leq z \leq 1.4$  as cluster galaxies. The lower cut,  $z = 0.96$ , was chosen in order not to include the very bright ( $K'_{AB} = 19.2$ ) but blue ( $I_{AB} - K'_{AB} = 1.42$ ) galaxy with an estimated redshift of 0.95, which is likely to be a foreground galaxy. Thirty-five out of the total 139 galaxies fall in the range of  $z = 0.96$ –1.4 (filled circles). We regard those 35 galaxies as members of the 3C 324 cluster (hereafter cluster members). Note that even if we change the boundaries by  $\Delta z \sim 0.02$ , the total number of cluster members changes by at most 3, which does not significantly affect our results given in the next section. We find from figure 4 that the estimated photometric redshifts of the brightest members tend to concentrate at  $z = 1.3$ –1.4, slightly higher than the spectroscopic redshift of 3C 324 ( $z = 1.21$ ) and some surrounding galaxies ( $z = 1.15, 1.21$ ; Dickinson 1997b). This difference probably comes from a mismatch between the model SEDs and the observed colors;  $\Delta(I_{AB} - K'_{AB}) \sim 0.1$  corresponds to  $\Delta z \sim 0.1$  (See figure 11).

Figure 5 shows the differential number counts of galaxies in the 3C 324 field after removing the 35 cluster members. The symbols are the same as in figure 3. The counts corrected for incompleteness are fairly consistent with those of the general fields at  $K'_{AB} < 22$ . Note, however, that the 3C 324 counts at  $K'_{AB} > 22$  are lower than the average of general fields. These may be due to a field variation, as discussed in subsection 3.2.

We checked the stability of our photometric redshift derived from the HYPERZ package against the photometric errors as follows. First, we made a mock catalog of 1000

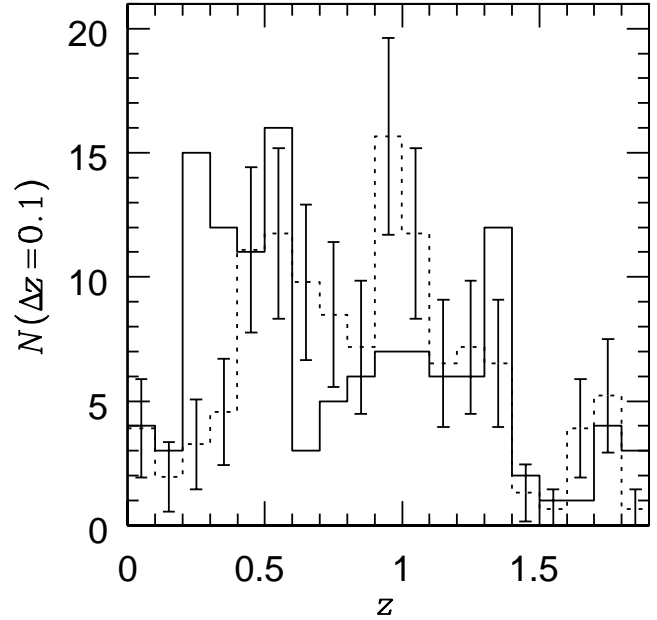


**Fig. 6.** Distribution of the estimated photometric redshifts for the  $K'_{AB} < 24$  galaxies (solid line). For a comparison, the observed redshift distribution of field galaxies with  $K'_{AB} < 24$  in the HDF is also plotted (dashed line) with the  $1\sigma$  Poisson errors. The redshift distribution of the HDF is normalized so that the number of galaxies is the same as of our 3C 324 field.

galaxies for each of the magnitude bins of  $\Delta m = 0.5$  mag in  $K'_{AB} = 18$ –24 mag at  $z = 1.2$  using a code provided in HYPERZ for the same bandpasses and limiting magnitudes as for the 3C 324 data. The generated galaxies are among the model ‘template’ galaxies used for estimating the photometric redshifts, and were randomly adopted from the 8 models (E to Im). We then applied HYPERZ to those galaxies to estimate the photometric redshifts. We found that about 80% of the galaxies with  $K'_{AB} < 23$  fall in the range  $0.96 \leq z \leq 1.4$ , implying that the criterion for membership adopted in this paper is appropriate. We found, however, that only  $\simeq 50\%$  of the faint ( $23 \leq K'_{AB} \leq 24$ ) galaxies satisfy this criterion, because of large photometric errors. Therefore, we treat galaxies with  $K'_{AB} > 23$  carefully in the following sections. We also checked the fraction of  $z > 2$  galaxies with the catalog of the Hubble Deep Field (HDF; Williams et al. 1996), whose redshifts were estimated with a photometric-redshift technique by Fernández-Soto, Lanzetta, and Yahil (1999). We found that the fraction is about 6% at  $K'_{AB} < 23$ , and about 13% at  $K'_{AB} < 24$ . Therefore, the contamination of  $z > 2$  galaxies is negligible at  $K'_{AB} < 23$ . However, at  $23 < K'_{AB} < 24$  the contamination can be a problem. It is worth noting that the blue galaxy fraction of cluster members, which we discuss in subsection 5.4, was derived from galaxies at  $K'_{AB} < 23$ , and thus the uncertainty in the photometric-redshift technique is not very large.

To estimate the field contamination, we compared the redshift distribution of the 3C 324 field with those of the HDF. Figure 6 shows the estimated photometric redshifts

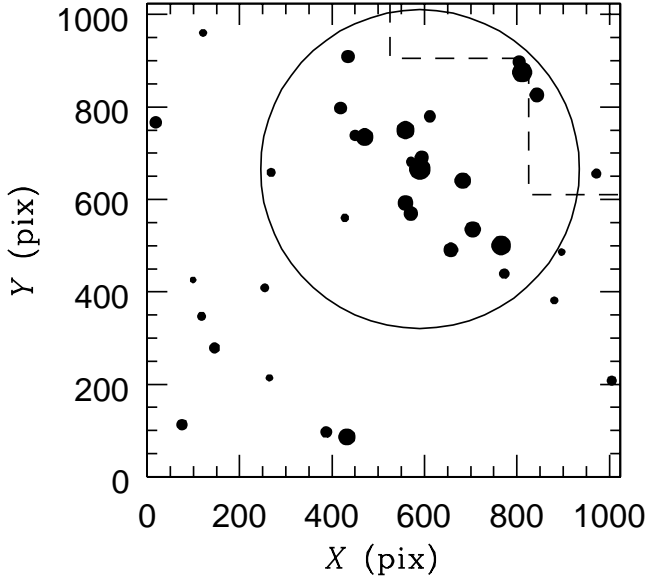


**Fig. 7.** Distribution of the 35 cluster members on the sky. The areas of filled circles are in proportion to the brightness of galaxies. The dashed line shows the boundary of the field of the HST observation. The large circle indicates the ‘inner region’.

(solid line) for the  $K'_{AB} < 24$  galaxies. As a reference, the observed redshift distribution of field galaxies with  $K'_{AB} < 24$  in the HDF is also plotted (dashed line) with the  $1\sigma$  Poisson errors. Note that most of the redshifts of the HDF galaxies were estimated by the photometric-redshift technique, but with a different code (Fernández-Soto et al. 1999). The redshift distribution of the HDF was normalized so that the number of galaxies would be the same as that of our 3C 324 field. We find from figure 6 that the field contamination expected from the HDF at  $0.96 < z < 1.4$  is significant. However, we should note that the galaxies in the 3C 324 field which are assigned photometric redshifts in the range  $0.96 < z < 1.4$  mostly have  $20 < K'_{AB} < 24$ . And at this magnitude range, the number counts of the field galaxies toward the 3C 324 cluster are systematically lower than the average, as shown in figure 5, possibly by up to a factor of 3. Therefore, we cannot estimate the field contamination precisely.

## 5. Results

### 5.1. Distribution of Member Galaxies

Figure 7 shows the distribution of the cluster members on the sky. The areas of the filled circles are in proportion to the brightness of the galaxies. The dashed line shows the boundary of the field of the HST observation. For the two galaxies outside the HST field, we used only V, I, and  $K'$  data to estimate their redshifts. We divided the observed field into the following two regions: the ‘inner’ region, which is enclosed by a circle of  $40''$  radius centered at 3C 324 (the large circle in figure 7 and figure 2), and the adjacent ‘outer’ region, which is the remaining region. A radius of  $40''$  corresponds to 0.33 Mpc at  $z = 1.2$  for

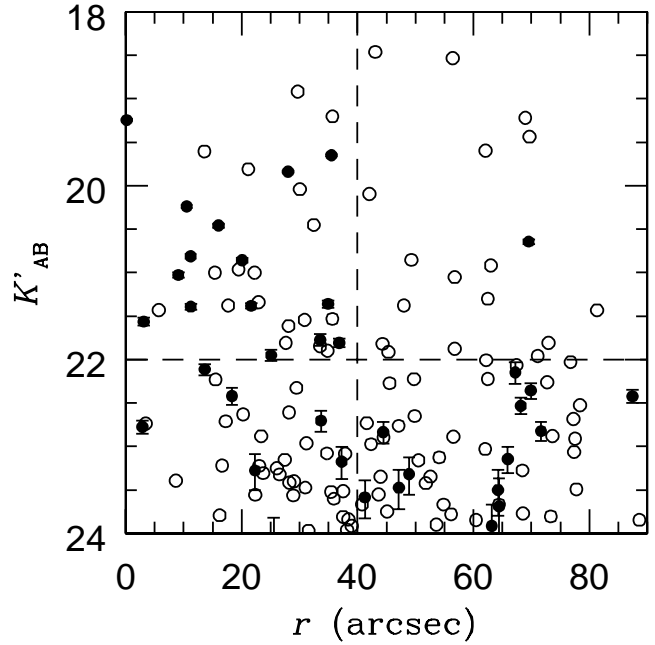


**Fig. 8.**  $K'_{AB}$  magnitude of galaxies against the distance in arcsecs from 3C 324. The filled and open circles indicate cluster members and non-members, respectively.

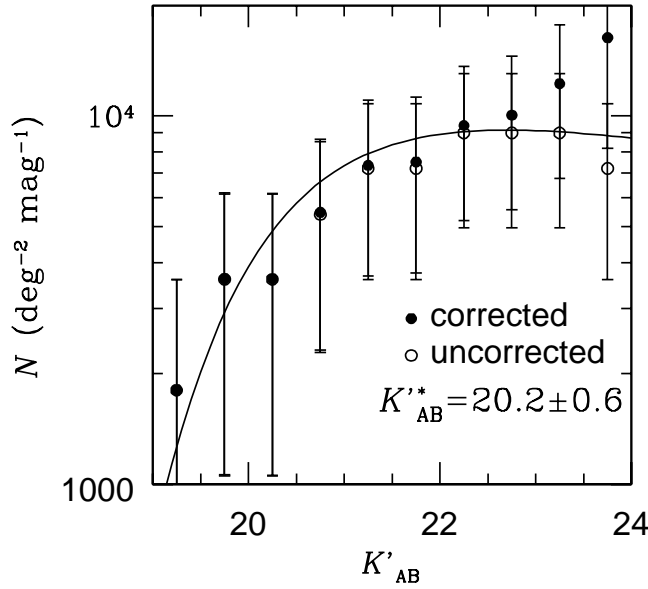
$\Omega_0 = 0.3$ ,  $\lambda_0 = 0.7$ ,  $h = 0.7$  cosmology. The areas of the inner and outer regions are  $1.40 \text{ arcmin}^2$  and  $2.60 \text{ arcmin}^2$ , respectively. A total of 21 galaxies among the 35 cluster members are in the inner region and 14 are in the outer region. Therefore, the number density of cluster galaxies is  $15.0 \text{ arcmin}^{-2}$  and  $5.4 \text{ arcmin}^{-2}$ , respectively.

Figure 8 plots  $K'_{AB}$  magnitude of galaxies against the distance from 3C 324. It is clear that the brighter galaxies are more centrally concentrated. The filled and open circles indicate the cluster members and field galaxies, respectively. Note that the distribution of the field galaxies is quite uniform, which gives indirect support that our photometric redshift estimation is successful. It is found that most (15/16) of the members with  $K'_{AB} < 22$  are located in the inner region. This is in contrast to the distribution of the faint ( $K'_{AB} \geq 22$ ) members. The number (number density) of the  $K'_{AB} \geq 22$  galaxies in the inner region and the outer regions are 6 (4.3 galaxies  $\text{arcmin}^{-2}$ ) and 13 (5.0 galaxies  $\text{arcmin}^{-2}$ ), respectively. The significant difference in the distributions of bright and faint members suggests a strong luminosity segregation of galaxies in the 3C 324 cluster.

### 5.2. Luminosity Function

Figure 9 shows the  $K'$ -band luminosity function of the cluster galaxies. The open and filled circles indicate the raw counts and those corrected for incompleteness, respectively. We fit the Schechter function,  $\phi(L) = \phi^*(L/L^*)^\alpha \exp(-L/L^*)$ , to the completeness-corrected counts in the range 19–23 mag in order to compare the results with those obtained in a similar manner for lower redshift clusters by de Propris et al. (1999). We fixed





**Fig. 9.**  $K'$ -band luminosity function of the cluster galaxies. The open and the filled circles indicate the raw counts and the counts corrected for incompleteness, respectively. The best-fitted Schechter function is plotted as the solid curve.

the faint-end slope of the Schechter function to  $\alpha = -0.9$  following de Propriis et al. (1999). We obtained the characteristic magnitude of  $K'^*_{AB} = 20.2 \pm 0.6$  mag. The fitted Schechter function is shown by the solid curve in figure 9. The corrected 3C 324 counts are slightly higher than the fitted Schechter function at the faint end ( $K'_{AB} > 23$ ). These high counts could be due to dwarf galaxies, because dwarf galaxies start to dominate at  $\sim M^* + 3$  mag in the  $K$ -band luminosity function of the nearby Coma cluster (de Propriis et al. 1998). However, the uncertainty of the counts at such faint magnitudes is large.

Our luminosity function was fitted very well by a Schechter form all the way down to a magnitude of at least  $K'_{AB} \sim 23$ . K00a claimed an abrupt decrease in their  $K'$ -band luminosity function of the galaxies in the inner region at  $K'_{AB} \gtrsim 22$ . They obtained the result by subtracting the galaxy counts in the general field or those in the outer region of the cluster from the raw counts in the inner region. K00a suggested two possible interpretations for the abrupt decrease: a strong luminosity segregation between the inner region and the outer region, or an intrinsic deficiency of faint galaxies in the 3C 324 cluster as a whole. Now, we find clearly that this decrease (in the  $K'_{AB} \gtrsim 22$ ) is due to luminosity segregation. With the photometric-redshift selected sample, we indeed see several faint cluster members with  $K'_{AB} \gtrsim 22$ , even in the inner region, which implies that the field subtraction in K00a using the average counts was also an overestimation, and that the true background counts in this region seems to be lower than the average of the general field.

Figure 10 compares the  $K^*_{AB}$  value of the 3C 324 cluster with those of lower-redshift clusters studied by de Propriis et al. (1999). Note that we transformed our  $K^*_{AB}$

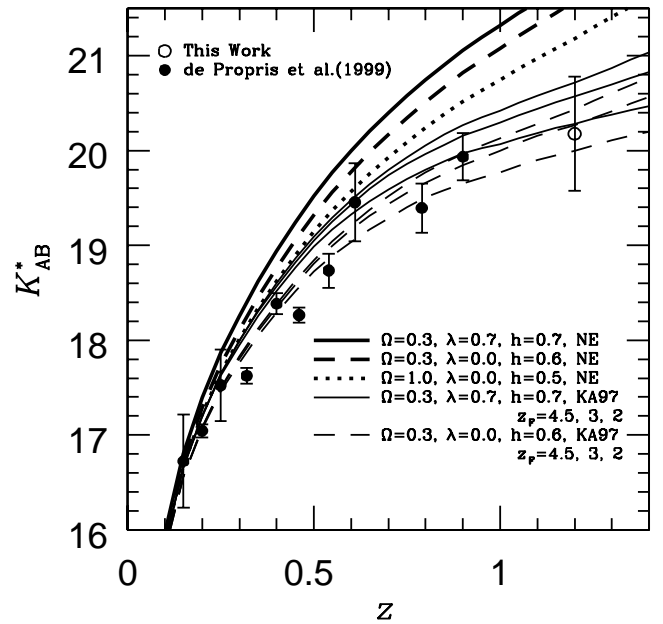


**Fig. 10.**  $K^*$ - $z$  Hubble diagram for the clusters at  $0.1 < z < 0.9$  studied by de Propriis et al. (1999; filled circles) and the 3C 324 cluster (open circle). Various lines show the behavior expected for no-evolution and passive evolution models with various cosmological parameters.  $z_F$  is the formation redshifts, and NE means no evolution.

to  $K^*_{AB}$  in this figure to be consistent with de Propriis et al. (1999). Various lines show the expected loci of the no-evolution and passive evolution models with various cosmological parameters calculated using Kodama and Arimoto's (1997; KA97) stellar population synthesis model. It is seen that our result follows the trend of the intermediate-redshift clusters, which is consistent with the passive-evolution models. Accordingly, at  $K'_{AB} \lesssim K^*_{AB}$  mag, the dominant population in the 3C 324 cluster seems to be old quiescent galaxies, which were formed at least  $\sim 1$  Gyr prior to the observed epoch.

### 5.3. The Color Properties

#### 5.3.1. Color-magnitude diagrams

Figure 11 shows the color-magnitude diagrams of the cluster members [(a)  $R_{F702W,AB} - K'_{AB}$  versus  $K'_{AB}$ , (b)  $I_{AB} - K'_{AB}$  versus  $K'_{AB}$ ]. The filled circles indicate the cluster members, and the small open circles indicate non-members. The filled square in each panel shows 3C 324, and the long-dashed line in each panel shows the  $3\sigma$ -detection limit of  $R_{F702W,AB}$  and  $I_{AB}$ , respectively. The solid line shows a predicted color-magnitude relation at the cluster redshift ( $z = 1.2$ ) for passively evolving galaxies formed at  $z_F = 4.5$  (KA97). This model assumes that the color-magnitude relation is a pure metallicity sequence as a function of the galaxy luminosity, and calibrates the relation by using that of Coma early-type galaxies (hereafter 'Coma C-M model'). In figure 11a, it is found that bright 8 galaxies (marked with circles) represent a tight color-magnitude relation (or so-called 'red finger'). The short-dashed line in each panel shows a linear regression

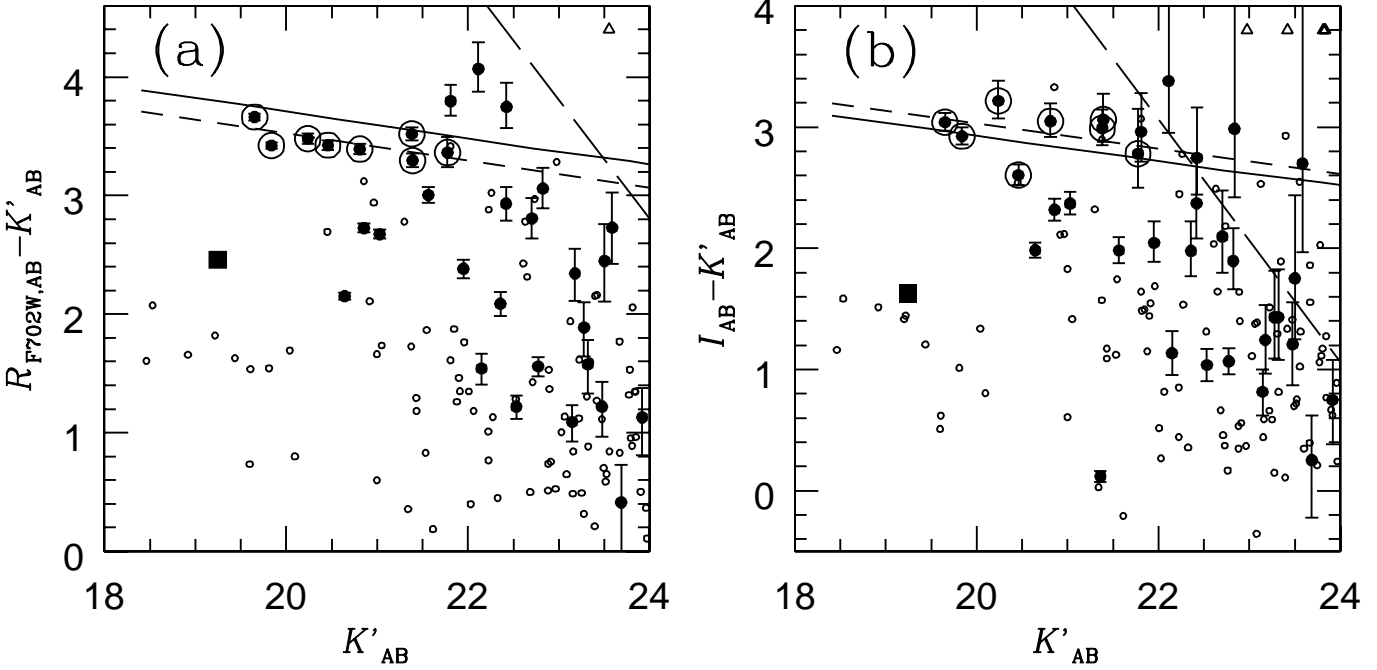


**Fig. 11.** Color-magnitude diagrams of the cluster members [(a)  $R_{F702W,AB} - K'_{AB}$  versus  $K'_{AB}$ , (b)  $I_{AB} - K'_{AB}$  versus  $K'_{AB}$ ]. The filled circles indicate cluster members, and the small open circles indicate non-members. The filled square in each panel shows 3C 324, and the long-dashed line in each panel shows the  $3\sigma$ -detection limit of  $R_{F702W,AB}$  and  $I_{AB}$ , respectively. The solid line corresponds to a predicted color-magnitude relation of passively evolving galaxies formed at  $z_F = 4.5$ . Eight bright galaxies, which make a tight color-magnitude relation, are indicated by a circles. The short dashed line in each panel shows a fit of a straight line to these 8 galaxies with its slope fixed to that of the model prediction.

line to these red-finger galaxies with the slope fixed to that of the model prediction. The color differences between the model line and the fitted line are  $-0.183$  mag and  $0.103$  mag for (a) and (b), respectively. We find that the scatters of red-finger galaxies around the best-fitted lines are  $0.091$  mag and  $0.193$  mag for (a) and (b), respectively. The scatter for (a) is comparable with those of the clusters at  $z < 0.9$  given in Stanford et al. (1998), who estimated the dispersion in the color-magnitude relation to be as small as  $0.1$  mag for the morphologically selected early-type galaxies in clusters. The scatter for (b), however, is twice as large as that for (a). This may be due to the relatively large photometric errors of the  $I$ -band image whose quality is not as good as the  $R_{F702W}$ -band image.

Note that the overall color distribution of the entire cluster members is broad by extending toward bluer colors. Similar trends are also seen in several clusters at high redshift (Stanford et al. 1997; Postman et al. 1998; Tanaka et al. 2000; van Dokkum et al. 2000). This suggests that there are more star-forming galaxies in clusters at  $z \gtrsim 1$  than in clusters at intermediate redshifts. We discuss this trend again in subsection 5.4. It is also worth noting that most of the relatively blue galaxies are faint:  $K'_{AB} > K'^*_{AB} + 1.5$ . Therefore, the major star formation of the bright galaxies ( $K'_{AB} \sim K'^*_{AB}$ ) was over at  $z = 1.2$ , as described in subsection 5.2, while the star formation activity of the faint galaxies was still considerable in the

3C 324 cluster at  $z \sim 1.2$ .

K00b extracted early-type member galaxies in the 3C 324 cluster using  $R_{F702W} - K'$  and  $B_{F450W} - R_{F702W}$  colors. They regarded a galaxy of a given  $R_{F702W} - K'$  as a member if it is redder in  $B_{F450W} - R_{F702W}$  than a model galaxy having the same  $R_{F702W} - K'$  color. They obtained two main results concerning the color-magnitude relation of early-type galaxies. Firstly, they found that the color-magnitude sequence is truncated at  $K'_{AB} \sim 22$ . We also find the truncation clearly in figure 11a. It is in remarkable contrast with the sequence of low-redshift clusters, which extend over more than 4 magnitudes (See also K00b). This may suggest that the faint ( $K'_{AB} \gtrsim K'^*_{AB} + 1.5$ ) early-type galaxies did not form until  $z \sim 1.2$ .

Secondly, K00b found that the early-type galaxies seem to form a broad color-magnitude sequence whose slope is much steeper than that predicted by coeval passive-evolution models (see figure 9 of K00b), especially at the faint end of  $K'_{AB} > 22$ . They suggested a possible interpretation for this aspect, that the ‘tilt’ of the slope is due to the age difference along the sequence; i.e., fainter galaxies are younger than brighter galaxies. We have confirmed that the slope of the red-finger-galaxies sequence ( $K'_{AB} < 22$ ) is consistent with that predicted by coeval passive-evolution models (Dickinson 1995; Kodama et al. 1998; K00b), but do not clearly confirm the sequence of red galaxies at  $K'_{AB} > 22$ , which makes the slope significantly steeper over the whole magnitude range in K00b.

Indeed, we find only three member galaxies on the blue side of the red sequence at  $K'_{AB} = 22$ –23, where K00b classified more galaxies as cluster members by their color selection. In this sense, there is no clear age-difference effect seen in the color–magnitude sequence of red galaxies.

Van Dokkum et al. (2001) investigated the color–magnitude relation of the cluster RXJ 0848+4453 at  $z = 1.27$ . They found that the color–magnitude relation of early-type galaxies in this cluster is shallower than that for the nearby Coma cluster, and deduced that the brightest early-type galaxies may have young stellar populations at  $z = 1.27$ . However, we do not find such a trend in the 3C 324 cluster. There might be a variation in the slope of the color–magnitude relation among clusters at  $z \sim 1.2$ .

### 5.3.2. Distribution of redder galaxies

Figure 12 shows the color deviation from the red color–magnitude sequence as a function of the projected distance from 3C 324 for all galaxies. The large filled circles indicate the cluster members with  $K'_{AB} < 23$ , while the faint cluster members with  $K'_{AB} > 23$  are shown as large open circles (since uncertainties in the photometric redshifts for the faint galaxies may be large due to their large photometric errors). The small open circles indicate the non-members. The large circles enclosing the large filled circles indicate the red-finger galaxies defined in figure 11, and the solid square in each panel shows the 3C 324 galaxy. We find that the red cluster members are highly concentrated in the inner region, while the bluer ones are more widely distributed. We refer to this as ‘color segregation’ analogous to the ‘luminosity segregation’ found in subsection 5.1. Since the bright and red galaxies are likely to be early-type galaxies (as in the lower redshift clusters), the ‘color segregation’ and the ‘luminosity segregation’ may be reflecting the morphology segregation or morphology–density relation discussed by Dressler (1980) and Dressler et al. (1997) that the early-type galaxies are concentrated towards the cluster center. The bright early-type galaxies at  $K'_{AB} < 22$  ( $\sim K'_{AB} + 2$ ) might have been formed near the cluster center. Note that the color distribution of the field galaxies is quite uniform against the distance from 3C 324, similar to the magnitude distribution shown in figure 8, which again supports our separation of field galaxies based on the photometric redshifts.

It is also worth pointing out that the physical scale of  $40''$  at  $z = 1.2$  is very small (0.33 Mpc). The early-type galaxies in the local clusters are usually distributed over  $\sim 1$  Mpc from the cluster center (e.g., Godwin et al. 1983 [Coma cluster]), and those of the MS 1054 cluster at  $z = 0.83$  are also distributed over  $\sim 1$  Mpc (See figure 10 of van Dokkum et al. 2000). This suggests that the 3C 324 cluster is more compact in size compared with the local clusters, and possibly to the clusters at intermediate redshifts.

### 5.3.3. 2-color diagram

In figure 13, we show an  $I_{AB} - K'_{AB}$  versus  $R_{F702W,AB} - I_{AB}$  diagram. The meanings of the symbols are the same as in figure 12. The solid line shows the evolutionary track

from  $z = 0$  to 2 of the Coma C–M model for  $M_V = -22$ . The effect of reddening is shown as arrows in the bottom-right corner, using the extinction curve of Calzetti et al. (2000). We find that only a few cluster galaxies are consistent with the Coma C–M model at  $z = 1.2$ . The eight red-finger galaxies (marked with large open circles) have significantly bluer ( $R_{F702W,AB} - I_{AB}$ ) colors than the Coma C–M models. Since the  $(R_{F702W,AB} - I_{AB})$  color approximately corresponds to  $(U - B)$  color in the rest frame at  $z = 1.2$ , we call these galaxies ‘UV-excess galaxies’. Note that these UV-excess galaxies have optical ( $I_{AB} - K'_{AB}$ ) colors which are consistent with the Coma C–M model.

Although there are four cluster members which have abnormally red  $R_{F702W,AB} - I_{AB}$  colors ( $R_{F702W,AB} - I_{AB} > 0.9$ ), we think that these colors are likely to be due to photometric errors. Two of them are located near to the edges of the images, where the image quality is worse than in the other part, especially in the  $I$ -band images where the fringe patterns could not be completely removed. The remaining two galaxies are located near a bright star or the 3C 324 galaxy where the accurate photometry is difficult.

To understand the nature of the UV-excess galaxies, we considered the disk models and the burst models, as follows. We added a disk or a star-burst onto the passively evolving galaxy (bulge component). The rest-frame near-UV colors ( $R_{F702W} - I$  at  $z \sim 1.2$ ) of these model galaxies were determined by the ratio of the disk or the star-burst component to the bulge component. As the disk component, we adopted a continuous star-formation model with an exponentially decaying time scale of 5 Gyr. As the star-burst component, we adopted a constant star-formation rate (SFR) model observed at 0.1 Gyr after the onset of star formation. Both of these models were calculated using the population synthesis code of KA97 with the Salpeter IMF (mass cutoffs  $M_l = 0.1M_\odot$ , and  $M_u = 60M_\odot$ ). For convenience, we introduced the disk and burst ratios,  $f_{\text{disk}}$  and  $f_{\text{burst}}$ , respectively, which are defined here as the flux ratio of the disk or burst component to the whole galaxy in the rest-frame  $B$  band. We changed  $f_{\text{disk}}$  and  $f_{\text{burst}}$  in the range of 0 and 1.

In figure 13, the disk and burst models are shown as the short-dashed line and the long-dashed line, respectively. Most of the member galaxies at  $I_{AB} - K'_{AB} < 2.6$ , which are probably late-type galaxies, follow the model track from the pure passively-evolving model to the pure disk or the star-burst model. Thus, the broad color distribution of the galaxies in the cluster region can be explained by a variation of the fraction of the disk or star-burst component in galaxies. The red galaxies at  $I_{AB} - K'_{AB} > 2.6$ , however, cannot be explained by these model tracks. It is worth noting that the fraction of such objects is very high in this cluster. Among the galaxies with  $K'_{AB} < 23$  and  $I_{AB} - K'_{AB} > 2.6$ ,  $\sim 60\%$  show UV excess. The mean of  $R_{F702W,AB} - I_{AB}$  color of these UV-excess galaxies is  $\sim 0.35$  mag bluer than that of the passively evolving galaxy with a similar  $I_{AB} - K'_{AB}$  ( $\sim 3.0$ ), and this difference is much larger than the photometric errors in  $R_{F702W}$  and  $I$  magnitudes. It is also worth noting that similar results were obtained by Tanaka et al. (2000) for a  $z \sim 1.1$

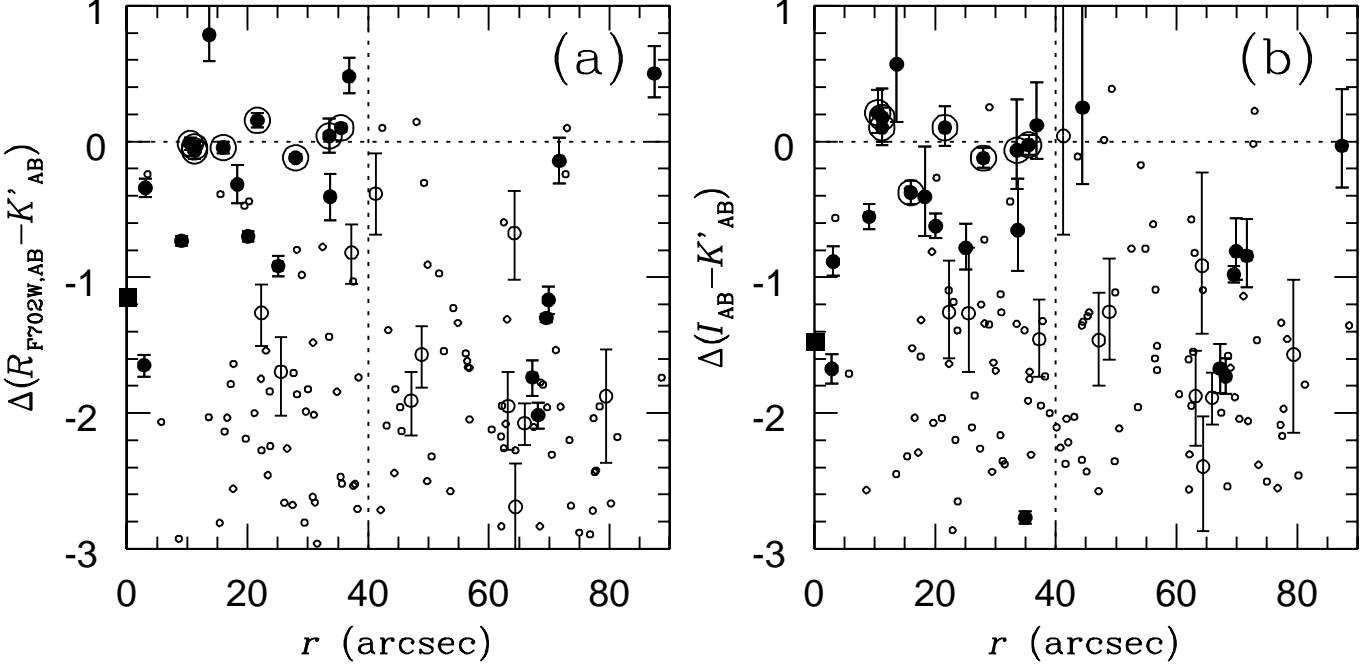


**Fig. 12.** Relation between the ‘differential color’ and the projected distance from 3C 324 for all galaxies, where differential color is defined as the observed color minus the color of the red sequence (long-dashed lines in figure 11) at the same  $K'$  magnitude. The large filled circles indicate the cluster members at  $K'_{AB} < 23$ , while the faint cluster members at  $K'_{AB} > 23$  are shown as open circles. The small open circles indicate the non-members. The red-finger galaxies defined in figure 11 are indicated by circles, and the solid square in each panel corresponds to 3C 324.

cluster and by Haines et al. (2001) for a  $z \sim 1.2$  cluster.

The existence ‘UV-excess galaxies’ suggests that a residual star formation might occur in the early-type galaxies at  $z \sim 1.2$ , although the possibility of a high star forming activity is ruled out in subsection 5.2 based on the evolution of  $K_{AB}^*$ . However, we find in the following that even the burst models cannot explain their blue  $U - V$  colors. Tanaka et al. (2000) suggested two possibilities for interpreting these UV-excess galaxies: an intermittent star formation or the last stage of the tail of star formation. To examine these possibilities, we computed another burst model for which a star-burst component has a flatter IMF ( $x = 0.35$ ) than the Salpeter IMF ( $x = 1.35$ ). We find that differences in  $R_{F702W,AB} - I_{AB}$  are less than 0.1 mag between the  $x = 0.35$  model and the Salpeter IMF model, implying that it is difficult to explain the UV-excess galaxies by flat IMF models. If we want to explain these UV-excess galaxies with an additional star formation in the red galaxies, we must introduce a very exotic shape of IMF, which brightens only UV light and with almost no effect on optical light. It may seem possible, on the other hand, that the burst or disk models with dust extinction can explain UV-excess galaxies. However, in order to explain the tight sequence of the UV-excess galaxies seen in figure 13, we need fine tuning between  $f_{\text{burst}}$  or  $f_{\text{disk}}$  and  $E(B - V)$ . We have not identified what causes the observed UV excess.

#### 5.4. Blue Galaxy Fraction

There have been few attempts to extend measurements of the Butcher–Oemler effect (Butcher, Oemler 1978, 1984) beyond  $z \sim 0.5$ , primarily because the field contamination becomes severer at higher redshifts. We try to extend the study on the Butcher–Oemler effect to this very high redshift cluster at  $z = 1.2$  by reducing the field contamination using the photometric-redshift technique.

Butcher and Oemler (1984) defined the fraction of blue galaxies,  $f_B$ , which are bluer than the color–magnitude sequence of early-type galaxies by more than 0.2 magnitude in the rest-frame  $B - V$  color. They imposed a radial cut,  $R < R_{30}$ , the radius which contains 30% of the cluster population, and the magnitude cut,  $M_V < -20$  in the rest-frame. Note that they did not take into account the luminosity and color evolution of galaxies in the above definition of the blue galaxy fraction.

If we ignore luminosity evolution, the magnitude limit that is equivalent to the Butcher–Oemler limit of  $M_V = -20$  in the rest frame is  $K'_{AB} = 22.7$  for the 3C 324 cluster, and a difference of  $\Delta(B - V) = 0.2$  mag in the rest frame corresponds to  $\Delta(I_{AB} - K'_{AB}) \simeq 0.65$  in the observed frame at  $z = 1.2$ . Thus, we define  $f_B$  of the 3C 324 cluster to be the fraction of galaxies brighter than  $K'_{AB} = 22.7$  and bluer in  $I_{AB} - K'_{AB}$  than the red-finger sequence (long-dashed line in figure 11) by more than 0.65 mag in the whole region observed. The obtained value of  $f_B$  is  $0.39 \pm 0.28$ . We derived  $f_B$  using  $I_{AB} - K'_{AB}$ , not  $R_{F702W,AB} - K'_{AB}$ ,



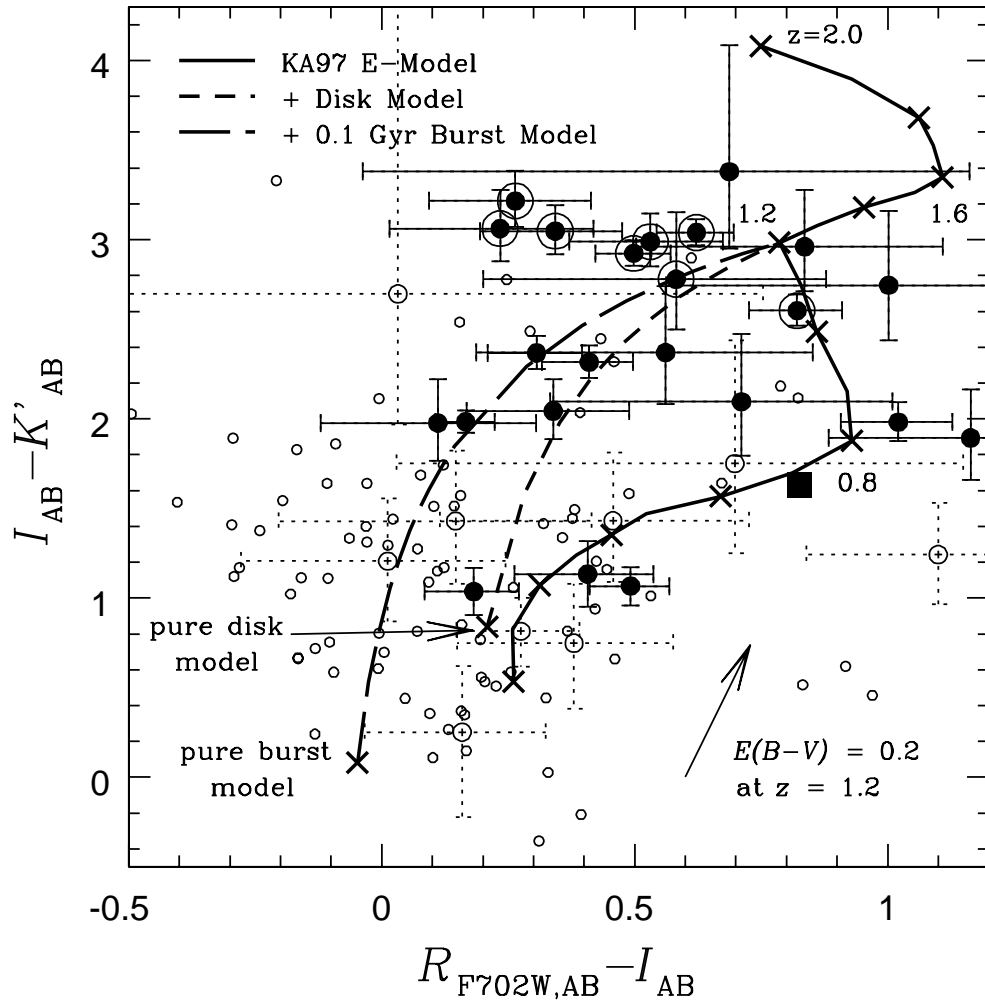


**Fig. 13.**  $R_{F702W,AB} - I_{AB}$  versus  $I_{AB} - K'_{AB}$  of the objects detected in the 3C324 field. The meaning of symbols is the same as in figure 12. The solid line is a prediction of passively evolving galaxies at  $0 \leq z \leq 2$  ( $M_V = -22$ ) formed at  $z_F = 4.5$ . The disk and burst models are also shown as the short-dashed line and the long-dashed line, respectively. The effect of internal extinction is shown as arrows in the bottom-right corner. See text for details.

because at  $z = 1.2$  the  $I$  band is nearer to the  $B$  band in the rest frame than the  $R$  band and the  $R$ -band image taken with the HST does not cover the whole  $K'$ -band image.

However, ignoring the luminosity evolution may not be a good assumption at such a high redshift as  $z = 1.2$ . Indeed, if passive evolution is adopted,  $M_V = -20$  at  $z = 0$  corresponds to  $K'_{AB} = 21.7$  at  $z = 1.2$ , which is one magnitude brighter than that for no evolution. Therefore, we must derive the value of  $f_B$  while taking the luminosity evolution of the  $M_V$  and  $B - V$  color into account. To estimate the effect of evolution, we used a model of passively evolving galaxies. A difference of  $\Delta(B - V) = 0.2$  mag corresponds to  $\Delta(I_{AB} - K'_{AB}) = 0.39$  at  $z = 1.2$  if evolution is considered, and we find  $f_B$  to be  $0.46 \pm 0.34$ . This value coincides with the value for no evolution within error bars, i.e., the effect of the evolution on  $f_B$  is found to be small.

Figure 14 shows the blue fraction ( $f_B$ ) of rich clusters at various redshifts. The filled square and the filled cir-

cle represent our results with and without an evolutionary correction, respectively. The open circles indicate 7 CNOC clusters and the Coma cluster taken from Kodama and Bower (2001), and the open square is for MS 1054-03 at  $z = 0.83$  (van Dokkum et al. 2000). The two lines in figure 14 are linear extrapolations to higher redshifts of the observed evolution of  $f_B$  obtained by Butcher and Oemler (1984;  $0 < z < 0.5$ ; solid line) and Rakos and Schombert (1995;  $0 < z < 1$ ; dotted line). Although the  $f_B$  of the 3C 324 cluster is found to be higher than those of  $z < 1$  clusters, the extremely high fraction of blue galaxies found by Rakos and Schombert (1995) in clusters at  $z > 0.5$  ( $f_B \sim 0.8$  at  $z \sim 1$ ) is not confirmed in our study, similar to the results obtained by van Dokkum et al. (2000). The  $f_B$ -value of the 3C 324 cluster is consistent within the error with the extrapolation of the evolution obtained in Butcher and Oemler (1984). The observed area ( $\sim 1 \text{ Mpc} \times 1 \text{ Mpc}$ ) is probably smaller than a circle of radius  $R = R_{30}$  (typically  $\sim 1 h^{-1} \text{ Mpc}$  in the Butcher and Oemler 1984). This means that the value of  $f_B$  obtained in this

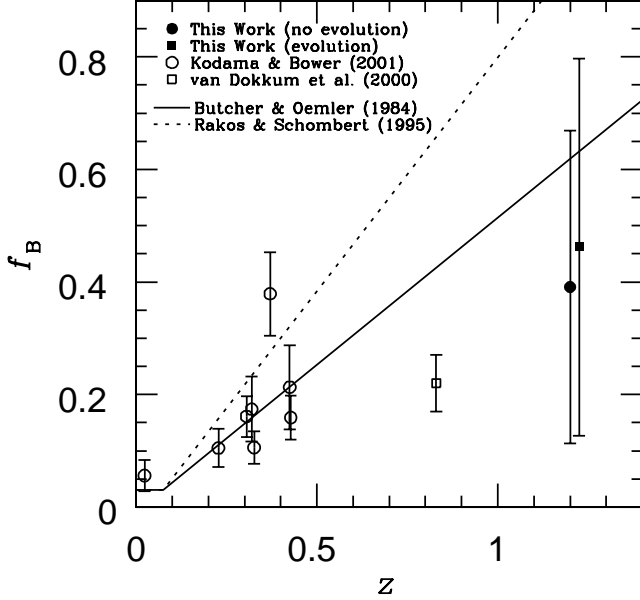


**Fig. 14.** Blue galaxy fraction  $f_B$  in rich clusters as a function of redshift. The filled square and circle show the result of this work with and without evolutionary correction, respectively. The open circles indicate 7 CNOC clusters and the Coma cluster, and the open square is for MS 1054-03 at  $z = 0.83$ . The two lines are extrapolations to higher redshifts of the observed evolution of  $f_B$  obtained by Butcher and Oemler (1984; solid line) and Rakos and Schombert (1995; dotted line).

work should be taken as the lower limit, because redder galaxies are more concentrated towards the cluster center. However, since the 3C 324 cluster is found to be compact in comparison with nearby rich clusters, we think  $f_B$  does not increase significantly, even if we exactly follow Butcher and Oemler's (1984) definition.

We find from figure 14 that the blue galaxy fraction,  $f_B = 0.39 \pm 0.28$ , of the 3C 324 cluster is higher than those of  $z < 1$  clusters. This suggests that the star-formation activity of the entire cluster members in the 3C 324 cluster is high compared with those of the intermediate clusters.

Note that the 3C 324 cluster is not necessarily a typical cluster at  $z \gtrsim 1$ . We have to observe more clusters at  $z \gtrsim 1$  to derive the general blue fraction at such a high redshift.

## 6. Summary

We have analyzed multi-photometric data of the cluster 3C 324 at  $z \simeq 1.2$  and have identified 35 galaxies as the cluster members with a photometric-redshift technique. We summarize our findings as follows:

1. The red and luminous galaxies are distributed in a region enclosed within a circle of  $40''$  (0.33 Mpc) radius from 3C 324, while bluer galaxies are distributed more or less uniformly over a wider area. This probably demonstrates morphology segregation. The giant early-type galaxies might have been formed near the cluster center. The concentration of early-type galaxies in such a small region

of  $r = 0.33$  Mpc suggests that the 3C 324 cluster is more compact in size compared with local clusters, and possibly to clusters at intermediate redshifts in which early-type galaxies generally extend over  $\sim 1$  Mpc.

2. The luminosity function of the cluster members is well fitted by a Schechter function, and the derived characteristic magnitude is  $K_{AB}^* = 20.2 \pm 0.6$  mag. We compared this value with  $K_{AB}^*$  of the lower-redshift clusters studied by de Propris et al. (1999), and we found that our result, together with those by de Propris et al. (1999), is consistent with the passive evolution models. This suggests that the giant early-type galaxies ( $\gtrsim K^* + 1$ ) are old quiescent galaxies which were formed at least  $\sim 1$  Gyr prior to the observed epoch.
3. We confirmed the tight color-magnitude sequences of the bright galaxies with  $19.5 < K_{AB} < 22$  in both  $R_{F702W,AB} - K'_{AB}$  versus  $K'_{AB}$  and  $I_{AB} - K'_{AB}$  versus  $K'_{AB}$  diagrams. The slope of the sequence is consistent with the passive evolution model. On the other hand, truncation of the color-magnitude sequence indicated by K00b is clearly seen at  $K'_{AB} \sim 22$ . It may suggest that the faint ( $K'_{AB} \gtrsim K_{AB}^* + 1.5$ ) early-type galaxies are still in the process of formation at  $z \sim 1.2$ .
4. The cluster contains members with blue colors at faint magnitudes. This is also observed in several other  $z \sim 1$  clusters. This suggests that although the bright galaxies have finished the major star formation, there are many faint galaxies ( $K'_{AB} \gtrsim K_{AB}^* + 2$ ) having star-forming activity at  $z \sim 1.2$ .
5. Most of the galaxies that have red  $I_{AB} - K'_{AB}$  colors are brighter in the rest UV (bluer in  $R_{AB} - I_{AB}$ ) compared with the passive evolution models. These UV-excess galaxies have also been found in other  $z > 1$  clusters. This suggests that cluster ellipticals show some residual star formation activity at  $z > 1$ .
6. We measured a fraction of blue cluster members following the definition of Butcher and Oemler (1984), which is  $f_B = 0.39 \pm 0.28$ . We compare this  $f_B$  value with those of other low-redshift clusters, and find that the 3C 324 cluster has a higher  $f_B$  than  $z < 1$  clusters. This suggests that the star-formation activity of the overall cluster members in this  $z \sim 1.2$  cluster is high compared with the clusters at intermediate redshifts.

A part of the data presented here were taken during a test observing run of the Subaru telescope. We are therefore indebted to all members of the Subaru Telescope, NAOJ, Japan. We would like to thank the engineering staffs of Mitsubishi Electric Co. and Fujitsu Co. for technical assistance during the observations. FN, MK, TK, HF, and MO acknowledge Japan Society for the Promotion of Science for support through its research fellowships for young scientists. This work was based in part on observations with the NASA/ESA Hubble Space Telescope, obtained from the data archive at the Space Telescope

Science Institute, U.S.A., which is operated by AURA, Inc. under NASA contract NAS5-26555.

## References

- Abraham, R. G., van den Bergh, S., Glazebrook, K., Ellis, R. S., Santiago, B. X., Surma, P., & Griffiths, R. E. 1996, *ApJS*, 107, 1
- Aragón-Salamanca, A., Ellis, R. S., Couch, W. J., & Carter, D. 1993, *MNRAS*, 262, 764
- Barger, A. J., Aragón-Salamanca, A., Ellis, R. S., Couch, W. J., Smail, I., & Sharples, R. M. 1996, *MNRAS*, 279, 1
- Benítez, N., Broadhurst, T., Rosati, P., Courbin, F., Squires, G., Lidman, C., & Magain, P. 1999, *ApJ*, 527, 31
- Bershady, M. A., Lowenthal, J. D., & Koo, D. C. 1998, *ApJ*, 505, 50
- Best, P. N. 2000, *MNRAS*, 317, 720
- Bolzonella, M., Miralles, J.-M., & Pelló, R. 2000, *ã*, 363, 476
- Bower, R. G., Kodama, T., & Terlevich, A. 1998, *MNRAS*, 299, 1193
- Bower, R. G., Lucey, J. R., & Ellis, R. S. 1992, *MNRAS*, 254, 601
- Bruzual, A. G., & Charlot, S. 1993, *ApJ*, 405, 538
- Butcher, H., & Oemler, A., Jr. 1978, *ApJ*, 219, 18
- Butcher, H., Oemler, A., Jr. 1984, *ApJ*, 285, 426
- Calzetti, D., Armus, L., Bohlin, R. C., Kinney, A. L., Koornneef, J., & Storchi-Bergmann, T. 2000, *ApJ*, 533, 682
- Couch, W. J., Barger, A. J., Smail, I., Ellis, R. S., & Sharples, R. M. 1998, *ApJ*, 497, 188
- Couch, W. J., & Sharples, R. M. 1987, *MNRAS*, 229, 423
- Cowie, L. L., Gardner, J. P., Hu, E. M., Songaila, A., Hodapp, K.-W., & Wainscoat, R. J. 1994, *ApJ*, 434, 114
- de Propriis, R., Eisenhardt, P. R., Stanford, S. A., & Dickinson, M. 1998, *ApJ*, 503, L45
- de Propriis, R., Stanford, S. A., Eisenhardt, P. R., Dickinson, M., & Elston, R. 1999, *AJ*, 118, 719
- Dickinson, M. 1995, in *ASP Conf. Ser. 86, Fresh Views of Elliptical Galaxies*, ed. A. Buzzini, A. Renzini, & A. Serrano (San Francisco: ASP), 283
- Dickinson, M. 1997a, in *the Hubble Space Telescope and the High Redshift Universe*, ed. N. R. Tanvir, A. Aragón-Salamanca, & J. V. Wall (Singapore: World Scientific), 207
- Dickinson, M. 1997b, in *The Early Universe with the VLT*, ed. J. Bergeron (Berlin: Springer), 274
- Djorgovski, S., Soifer, B. T., Pahre, M. A., Larkin, J. E., Smith, J. D., Neugebauer, G., Smail, I., Matthews, K., et al. 1995, *ApJ*, 438, L13
- Dressler, A. 1980, *ApJ*, 236, 351
- Dressler, A., & Gunn, J. E. 1992, *ApJS*, 78, 1
- Dressler, A., Oemler, A., Jr., Couch, W. J., Smail, I., Ellis, R. S., Barger, A., Butcher, H., Poggianti, B. M., & Sharples, R. M. 1997, *ApJ*, 490, 577
- Dressler, A., Smail, I., Poggianti, B. M., Butcher, H., Couch, W. J., Ellis, R. S., & Oemler, A., Jr. 1999, *ApJS*, 122, 51
- Ellis, R. S., Smail, I., Dressler, A., Couch, W. J., Oemler, A., Jr., Butcher, H., & Sharples, R. M. 1997, *ApJ*, 483, 582
- Fernández-Soto, A., Lanzetta, K. M., & Yahil, A. 1999, *ApJ*, 513, 34
- Gardner, J. P., Cowie, L. L., & Wainscoat, R. J. 1993, *ApJ*, 415, L9
- Gladders, M. D., López-Cruz, O., Yee, H. K. C., & Kodama, T. 1998, *ApJ*, 501, 571
- Godwin, J. G., Metcalfe, N., & Peach, J. V. 1983, *MNRAS*, 202, 113
- Haines, C. P., Clowes, R. G., Campusano, L. E., & Adamson, A. J. 2001, *MNRAS*, 323, 688
- Hall, P. B., & Green, R. F. 1998, *ApJ*, 507, 558
- Kajisawa, M., & Yamada, T. 1999, *PASJ*, 51, 719
- Kajisawa, M., Yamada, T., Tanaka, I., Maihara, T., Iwamuro, F., Terada, H., Goto, M., Motohara, K., et al. 2000a, *PASJ*, 52, 53 (K00a)
- Kajisawa, M., Yamada, T., Tanaka, I., Maihara, T., Iwamuro, F., Terada, H., Goto, M., Motohara, K., et al. 2000b, *PASJ*, 52, 61 (K00b)
- Kodama, T., & Arimoto, N. 1997, *A&A* 320, 41 (KA97)
- Kodama, T., Arimoto, N., Barger, A. J., & Aragón-Salamanca, A. 1998, *ã*, 334, 99
- Kodama, T., Bell, E. F., & Bower, R. G. 1999, *MNRAS*, 302, 156
- Kodama, T., & Bower, R. G. 2001, *MNRAS*, 321, 18
- Kristian, J., Sandage, A., & Katem, B. 1974, *ApJ*, 191, 43
- Kuntschner, H., & Davis, R. L. 1998, *MNRAS*, 295, L29
- Landolt, A. U. 1992, *AJ*, 104, 340
- Maihara, T., Iwamuro, F., Tanabe, H., Taguchi, T., Hata, R., Oya, S., Kashikawa, N., Iye, M., et al. 2001, *PASJ*, 53, 25
- McCracken, H. J., Metcalfe, N., Shanks, T., Campos, A., Gardner, J. P., & Fong, R. 2000, *MNRAS*, 311, 707
- McLeod, B. A., Bernstein, G. M., Rieke, M. J., Tollestrup, E. V., & Fazio, G. G. 1995, *ApJS*, 96, 117
- Metcalfe, M., Shanks, T., Fong, R., & Jones, L. R. 1991, *MNRAS*, 249, 498
- Minezaki, T., Kobayashi, Y., Yoshii, Y., & Peterson, B. A. 1998, *ApJ*, 494, 111
- Miyazaki, S., Sekiguchi, M., Imi, K., Okada, N., Nakata, F., & Komiyama, Y. 1998, *Proc. SPIE*, 3355, 363
- Morris, S., Hutchings, J. B., Carlberg, R. G., Yee, H. K. C., Ellingson, E., Balogh, M. L., Abraham, R. G., & Smecker-Hane, T. A. 1998, *ApJ*, 507, 84
- Motohara, K., Maihara, T., Iwamuro, F., Oya, S., Imanishi, M., Terada, H., Goto, M., & Iwai, J. 1998, *Proc. SPIE*, 3354, 659
- Moustakas, L. A., Davis, M., Graham, J. R., Silk, J., Peterson, B. A., & Yoshii, Y. 1997, *ApJ*, 475, 445
- O'Connell, R. W. 1988, in *Towards Understanding Galaxies at Large Redshift*, ed. R. G. Kron, & A. Renzini (Dordrecht: Kluwer), 177
- Oemler, A., Jr. 1974, *ApJ*, 194, 1
- Oemler, A., Jr., Dressler, A., & Butcher, H. R. 1997, *ApJ*, 474, 561
- Olsen, L. F., Scodreggio, M., da Costa, L., Slijkhuis, R., Benoist, C., Bertin, E., Deul, E., Erben, T., et al. 1999, *ã*, 345, 363
- Ostrander, E. J., Nichol, R. C., Ratnatunga, K. U., & Griffiths, R. E. 1998, *AJ*, 116, 2644
- Poggianti, B. M., Smail, I., Dressler, A., Couch, W. J., Barger, A. J., Butcher, H., Ellis, R. S., & Oemler, A., Jr. 1999, *ApJ*, 518, 576
- Postman, M., Lubin, L. M., Gunn, J. E., Oke, J. B., Hoessel, J. G., Schneider, D. P., & Christensen, J. A. 1996, *AJ*, 111, 615
- Postman, M., Lubin, L. M., & Oke, J. B. 1998, *AJ*, 116, 560

- Rakos, K. D., & Schombert, J. M. 1995, ApJ, 439, 47
- Rosati, P., Stanford, S. A., Eisenhardt, P. R., Elston, R., Spinrad, H., Stern, D., & Dey, A. 1999, AJ, 118, 76
- Saracco, P., D’Odorico, S., Moorwood, A., Buzzoni, A., Cuby, J.-G., & Lidman, C. 1999, *â*, 349, 751
- Saracco, P., Iovino, A., Garilli, B., Maccagni, D., & Chincarini, G. 1997, AJ, 114, 887
- Smail, I., & Dickinson, M. 1995, ApJ, 455, L99
- Soifer, B. T., Matthews, K., Djorgovski, S., Larkin, J., Graham, J. R., Harrison, W., Jernigan, G., Lin, S., et al. 1994, ApJ, 420, L1
- Spinrad, H., & Djorgovski, S. 1984, ApJ, 280, L9
- Stanford, S. A., Eisenhardt, P. R., & Dickinson, M. 1998, ApJ, 492, 461
- Stanford, S. A., Elston, R., Eisenhardt, P. R., Spinrad, H., Stern, D., & Dey, A. 1997, AJ, 114, 2232
- Tanaka, I., Yamada, T., Aragón-Salamanca, A., Kodama, T., Miyaji, T., Ohta, K., & Arimoto, N, 2000, ApJ, 528, 123
- van Dokkum, P. G., Franx, M., Fabricant, D., Illingworth, G. D., & Kelson, D. D. 2000, ApJ, 541, 95
- van Dokkum, P. G., Franx, M., Kelson, D. D., Illingworth, G. D., Fisher, D., & Fabricant, D. 1998, ApJ, 500, 714
- van Dokkum, P. G., Stanford, S. A., Holden, B. P., Eisenhardt, P. R., Dickinson, M., & Elston, R. 2001, ApJ, 552, L101
- Williams, R. E., Blacker, B., Dickinson, M., van Dyke Dixon, W., Ferguson, H. C., Fruchter, A. S., Giabalisco, M., Gilliland, R. L., et al. 1996, AJ, 112, 1335